Structural effects of a dimer interface mutation on catalytic activity of triosephosphate isomerase: The role of conserved residues and complementary mutations

3 authors, including:

Mousumi Banerjee
Indian Institute of Science Education and Research, Tirupati

16 PUBLICATIONS   158 CITATIONS

SEE PROFILE

Padmanabhan Balaram
Indian Institute of Science

595 PUBLICATIONS   19,813 CITATIONS

SEE PROFILE

Some of the authors of this publication are also working on these related projects:

Bioactive peptides View project

Design, construction and applications of peptide-based nano-materials View project

Structural effects of a dimer interface mutation on catalytic activity of triosephosphate isomerase

The role of conserved residues and complementary mutations

Mousumi Banerjee[1], Hemalatha Balaram[2] and Padmanabhan Balaram[1]

1 Molecular Biophysics Unit, Indian Institute of Science, Bangalore, India
2 Molecular Biology and Genetics Unit, Jawaharlal Nehru Centre for Advanced Scientific Research, Jakkur, Bangalore, India

The active site of triosephosphate isomerase (TIM, EC: 5.3.1.1), a dimeric enzyme, lies very close to the subunit interface. Attempts to engineer monomeric enzymes have yielded well-folded proteins with dramatically reduced activity. The role of dimer interface residues in the stability and activity of the *Plasmodium falciparum* enzyme, *Pf*TIM, has been probed by analysis of mutational effects at residue 74. The *Pf*TIM triple mutant W11F/W168F/Y74W (Y74W*) has been shown to dissociate at low protein concentrations, and exhibits considerably reduced stability in the presence of denaturants, urea and guanidinium chloride. The Y74W* mutant exhibits concentration-dependent activity, with an approximately 22-fold enhancement of k_{cat} over a concentration range of 2.5–40 μM, suggesting that dimerization is obligatory for enzyme activity. The Y74W* mutant shows an approximately 20-fold reduction in activity compared to the control enzyme (*Pf*TIM WT*, W11F/W168F). Careful inspection of the available crystal structures of the enzyme, together with 412 unique protein sequences, revealed the importance of conserved residues in the vicinity of the active site that serve to position the functional K12 residue. The network of key interactions spans the interacting subunits. The Y74W* mutation can perturb orientations of the active site residues, due to steric clashes with proximal aromatic residues in *Pf*TIM. The available crystal structures of the enzyme from *Giardia lamblia*, which contains a Trp residue at the structurally equivalent position, establishes the need for complementary mutations and maintenance of weak interactions in order to accommodate the bulky side chain and preserve active site integrity.

Structured digital abstract
- MINT-7137586: *TIM* (uniprotkb:Q07412) and *TIM* (uniprotkb:Q07412) *bind* (MI:0407) by *molecular sieving* (MI:0071)
- MINT-7137703, MINT-7137792: *TIM* (uniprotkb:Q07412) and *TIM* (uniprotkb:Q07412) *bind* (MI:0407) by *circular dichroism* (MI:0016)
- MINT-7137739: *TIM* (uniprotkb:Q07412) and *TIM* (uniprotkb:Q07412) *bind* (MI:0407) by *classical fluorescence spectroscopy* (MI:0017)

Introduction

The glycolytic enzyme triosephosphate isomerase occupies a central position in the development of structural and mechanistic enzymology [1–3]. As the first well-characterized protein exhibiting a $(\beta/\alpha)_8$ barrel fold [2], TIM has been a subject of extensive study over the past five decades [4–9]. The enzyme is a dimer in all organisms, with the exception of thermophilic archaebacteria, in which it exists as a tetramer [10–12]. The TIM dimer interface consists mainly of four loops [13]. TIM is an extremely tight dimer, with an estimated K_d value for the wild-type trypanosomal TIM of approximately 10^{-11} M [14]. The overall surface area buried at the dimeric interface of TIMs from diverse sources is approximately 1600–1800 $Å^2$ per subunit. In an early study using yeast TIM, Casal *et al.* examined N78T, N78I and N78D mutants. The mutants had an appreciably lower k_{cat} value and were significantly less stable at elevated temperatures and in the presence of denaturants and proteolytic agents [15]. Engineered monomeric TIM constructed from a mutant from which loop 3 had been deleted showed negligible activity, suggesting that dimerization may be important for both stability and function [13,14]. To establish the relationship between dimerization and catalytic activity, several site-directed mutants of various TIMs have been generated. An H47N variant of *Trypanosoma - brucei* TIM was found to form monomers at low protein concentration (≤ 3 mg·mL^{-1}), with considerable impairment of activity [16]. Similarly, the mutant T75G/G76R was also found to dissociate at low protein concentration, resulting in a 1000-fold reduction of activity [17]. The human TIM mutants R98Q and M14Q/R98Q showed enzyme inactivation as well as strongly affected subunit association [18].

Plasmodium falciparum triosephosphate isomerase (*Pf*TIM) has been the subject of study in our laboratory for a number of years [19]. Interest in this enzyme stems from the fact that the plasmodial enzyme exhibits unusual properties, especially with respect to the conformation of the active site loop [20] and differences in the nature of the dimer interface compared to the human enzyme. The fact that a cysteine residue is found at position 13 in the pathogens, compared to methionine in human enzyme, has stimulated studies involving selective inhibition using sulfhydryl-modifying reagents [21] in the TIMs from *Trypanosoma brucei*, *Trypanosoma cruzi* and *Leishmania mexicana* [22–24].

Previously, Tyr74 of *Pf*TIM was replaced by Cys in order to introduce a symmetry-related disulfide bond with the Cys residue at position 13 of the other subunit [25,26], yielding a covalently bridged dimer. The oxidized and reduced forms of the Y74C mutant had very different thermal stabilities. While the stability of the Y74C$_{ox}$ mutant was comparable to that of wild-type enzyme, the Y74C$_{red}$ mutant was very labile [26]. Thus it was concluded that the reduction in residue volume at position 74 at the dimer interface created a cavity, with consequent destabilization. Formation of the cavity and its consequences were further tested by introducing the smallest residue, glycine, at position 74. The Y74G mutant was considerably less stable than the wild-type enzyme at elevated temperature and in the presence of denaturants [27].

Extending these studies, we examine here the effect of increasing the bulk of the residue at position 74. Surprisingly, the Y74W mutant exhibited loss of both activity and stability. There was also evidence of dimer dissociation at low protein concentration. These results prompted us to re-examine the role of the dimeric structure in facilitating enzyme activity. Placement of an intrinsic fluorophore (tryptophan) at the dimer interface also provides the opportunity to monitor subunit dissociation by fluorescence methods. Figure 1 shows the environment of the Y74 residue of *Pf*TIM. Y74 appears in a cluster of aromatic residues that might be anticipated to contribute to dimer stability through favorable aromatic–aromatic interactions [27]. In order to examine the effect of introduction of additional atoms at position 74, we engineered a Y74W mutant of *Pf*TIM. The wild-type enzyme contains two tryptophan residues, W11 and W168. In order to simplify the interpretation of fluorescence spectra, we constructed a triple mutant of *Pf*TIM W11F/W168F/Y74W (Y74W*). Previous studies from this laboratory on the single mutants W11F and W168F have shown that the substitutions at these sites do not significantly impair enzyme activity [28]. Interestingly, the bulky Trp residue is found at this position in the sequence of TIM from *Giardia lamblia* (*Gl*TIM) whose molecular structure has also been determined [29]. A direct comparison of Y74 (in *Pf*TIM) and W75 (the Y74-equivalent residue in *Gl*TIM) revealed a set of complementary mutations in the near vicinity, which in turn help to accommodate the bulk of the tryptophan residue in *Gl*TIM without changing the overall stability or function.

Results

This study primarily focuses on the triple mutant W11F/W168F/Y74W (Y74W*), generated using a 'tryptophan-less' template W11F/W168F (WT*). This template was chosen in order to use the intrinsic
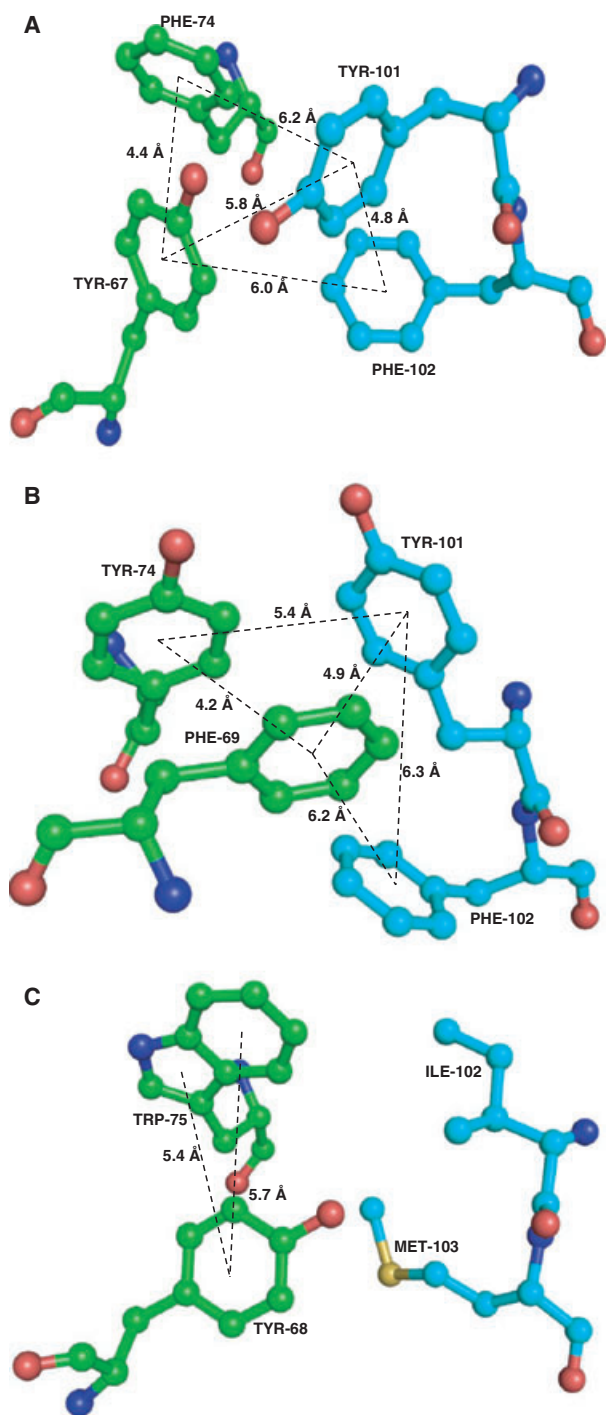
Fig. 1. The environment of residue 74 (and its structural equivalents) in *Pf*TIM, yeast and *Gl*TIM: side-chain cluster involving residues 69, 74, 101 and 102. (A) *Pf*TIM (Protein Data Bank code 1O5X; F69-Y74-Y101-F102), (B) yeast (Protein Data Bank code 1NEY; Y67-F74-Y101-F102), and (C) *Gl*TIM (Protein Data Bank code 2DP3; Y68-W75-I102-M103). The centroid to centroid distances are marked for all aromatic–aromatic pairs. The residues in green are from subunit A and those in cyan are from subunit B. The images were generated using PYMOL [57].

fluorescence of the engineered Trp74 residue to monitor dimer dissociation. All the mutant proteins were checked for homogeneity by SDS–PAGE (Fig. S1) and characterized by precise mass determination using LC-ESI mass spectrometry (ESI MS, Bruker Daltonics, Bremen, Germany) (Fig. S2).

Kinetic parameters

The enzymatic activity of the purified protein was measured using a coupled enzyme assay. The kinetic parameters for the mutant proteins are listed in Table 2, together with the relevant parameters for the WT protein and related mutants described previously. The Michaelis–Menten and Lineweaver–Burke plots for the enzymes are shown in Fig. S3. The W11F/W168F mutant (WT*) shows a twofold reduction in k_{cat} values compared to the *Pf*TIM wild-type. The W168F and W11F single mutants examined previously have activity comparable to that of the double mutant. However, the triple mutant Y74W* shows an approximately 20-fold reduction in k_{cat} compared to the WT* enzyme. There are two possible reasons for the low activity of the Y74W* mutant: (a) introduction of the bulkier residue at the interface in place of a tyrosine may destabilize the dimer, resulting in a shift in the equilibrium towards an inactive/less active monomeric form, or (b) insertion of the bulkier residue at the tightly packed interface may result in structural rearrangements at the proximal active site.

In order to address this issue, the dependence of activity on protein concentration was determined for the triple mutant Y74W*, the double mutant WT* and the wild-type (*Pf*TIM WT) enzymes. Enzyme activity was measured over a wide range of protein concentrations from 2.5 to 40 μM. It should be noted that the optimum concentration for the enzyme assay with the WT enzyme is 370 pM (10 ng·mL^{-1}); however, under these condition, the progress of the reaction for the triple mutant Y74W* is extremely slow, presumably because of the extremely low population of the catalytically competent dimeric species. Consequently, enzyme assays for the triple mutant were performed at much higher protein concentration (67.5 μg·mL^{-1}–1.08 mg·mL^{-1}; 2.5–40 μM). Under these conditions, the progress of the reactions of WT enzyme and other mutants is very fast. The results are summarized in Fig. 2. It is evident that the Y74W* mutant shows an enhancement of activity of 21.9-fold over the concentration range 2.5–40 μM, strongly suggesting that the loss of activity at low concentration may be attributed to subunit dissociation. In contrast, both the WT and WT* enzymes show no concentration dependence of specific activity, suggesting that these proteins retain their dimeric nature even at the lowest
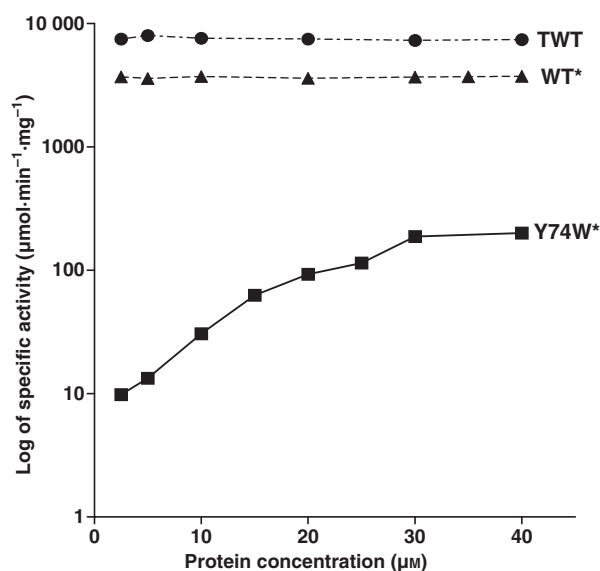
Fig. 2. Concentration-dependent enzyme activity of *Pf*TIM wild-type, the double mutant W11F/W168F (WT*) and the triple mutant W11F/W168F/Y74W (Y74W*). Assays of these three enzymes were carried out over a concentration range of 2.5–40 μM. The enzymes were incubated at the various concentrations in 100 mM triethanolamine/HCl (pH 7.6) for 1 h. All enzyme activity measurements were performed using the same buffer.

concentration examined. It is important to note that even at the highest concentration studied (40 μM), the Y74W* mutant does not reach the same level of activity as WT*.

Analytical gel filtration

Analytical gel filtration provides a direct means of assessing the oligomeric status of proteins. Figure 3 shows the gel filtration profiles obtained on an Super-dex-200 column for the triple mutant Y74W*. At a protein concentration of 40 μM, a single band is observed, with an elution volume of 13.9 mL, corresponding to a dimeric enzyme (54 kDa) with a subunit mass of 27 kDa. *Pf*TIM WT and WT* elute at exactly this position under similar conditions. However, at a much lower concentration of 5 μM, the gel filtration profile for the Y74W* mutant clearly shows two distinct species eluting at 13.9 and 15.3 mL. The later elution volume corresponds to the expected position for a monomeric protein with a mass of 27–28 kDa. In contrast, *Pf*TIM wild-type and WT* elute as a single peak centered at 13.9 mL, the position corresponding to the dimer, even at the lowest concentration studied. Inspection of the gel filtration profile in Fig. 3 shows that the peak corresponding to the monomeric species is considerably broader, presumably due to a distribution of partially

unfolded conformations. At a protein concentration of 5 μM, the monomeric species appears to predominate in the case of Y74W*. The gel filtration results indicate that the Y74W* mutant is dimeric at a concentration of 40 μM. However, at the highest concentration studied, there was an approximately 20-fold difference in the measured k_{cat} value for Y74W* compared to WT*, with the former being significantly less active. The activity measurements, together with the gel filtration results, suggest that, monomeric Y74W* possesses very low levels of activity, but complete activity is not regained even upon dimerization. Thus, position 74 is not only critical for the stability of the dimer, it may also be involved in maintaining the integrity of the active site. These results clearly suggest that the dimer interface in the Y74W* mutant is destabilized to a considerable extent.

Fluorescence spectroscopy

As seen from Fig. 1, the Y74 residue of one subunit makes close contact with Y101 and F102 of the other subunit. Thus, subunit dissociation in the case of the triple mutant Y74W* is expected to result in solvent exposure of the buried Trp74 residue. Figure 4 summarizes the dependence of the emission maxima (λ_{max}) on protein concentration for Y74W* and the *Pf*TIM WT protein. The wild-type protein shows no change in the emission wavelength of 332 nm over the protein concentration range 0.625–40 μM, but the Y74W* mutant shows a sharp dependence of emission wavelength on protein concentration. At the lowest concentration examined, 0.625 μM, the emission maximum is observed at 343 nm, with a shift to 336 nm at a protein concentration of 40 μM. The observed red shift on dilution is consistent with subunit dissociation, resulting in transfer of the Trp74 residue from a buried, hydrophobic environment to a polar aqueous environment. Further evidence for dimer dissociation in the Y74W* mutant can be obtained by examining the concentration dependence of the collisional quenching constant obtained from Stern–Volmer plots (Fig. 5) for the quencher acrylamide [30]. The effect of addition of acrylamide over the concentration range 100 mM–1 M was studied for protein concentrations ranging from 5 to 40 μM. In the case of the wild-type protein (*Pf*TIM WT), there is a very little concentration dependence of the quenching curves. In contrast, the quenching observed for the Y74W* mutant shows a pronounced concentration dependence, with a much greater degree of quenching at lower protein concentration. This is fully consistent with subunit dissociation resulting in a much greater accessibility to the quencher at concentrations < 10 μM. The quenching
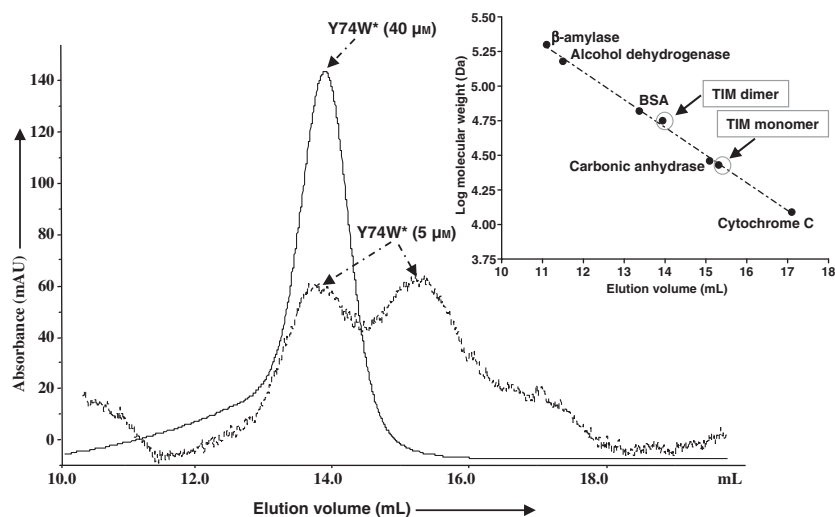
Fig. 3. Analytical gel filtration profiles for the triple mutant W11F/W168F/Y74W at two concentrations. The column used for gel filtration was a Superdex-200 (length 30 cm, internal diameter 10 mm. Buffer containing 20 mM Tris/HCl (pH 8.0) with 100 mM sodium chloride was used for all runs at a flow rate of 0.5 mL·min^{-1}. The inset shows the relative retention volumes of standard molecular weight markers.

curves at a protein concentration of 5 μM exhibit a significant deviation from linearity, suggestive of both static and dynamic quenching.

Stability to denaturants and temperature

The $(\alpha/\beta)_8$ barrel fold observed in TIMs is a robust structure that is incompletely denatured in urea solution. Previous studies of *Pf*TIM wild-type established that considerable secondary structure is maintained even in 8 M urea solution [25]. Guanidinium chloride is a more effective denaturant, yielding a C_m (mid-point of the unfolding curve) of approximately 2.4 M for *Pf*TIM WT. The protein also undergoes irreversible thermal melting and precipitates at 58 °C. Table 3 provides a comparison of the denaturation parameters of *Pf*TIM wild-type and the Y74W* triple mutant. For comparison, the measured parameters for the double mutant W11F/W168F and previously studied mutants are also summarized. It is immediately evident that the Y74W* mutant is considerably less stable in the presence of denaturants such as guanidinium chloride, and is also thermally more labile.

Discussion

Effects of the Y74W mutation

Residue 74, which lies at the dimer interface of PfTIM, appears to be important in promoting subunit dissociation [27] and also in maintaining the geometry of the active site. The availability of crystal structures of TIMs from 21 sources and the large database of TIM sequences from various sources facilitate an analysis of mutational effects. Most importantly, determination of the crystal structure of yeast TIM with the substrate

dihydroxyacetone phosphate [31] provides an excellent starting point for examining the consequence of mutations that may affect substrate binding and catalysis. Using a database of 380 unique TIM sequences from non-archaeal sources, we have examined the nature of substitutions at the position equivalent to residue 74 in *Pf*TIM. Archaeal TIMs were excluded as they have a shorter polypeptide length and are anticipated to form tetrameric structures, as already established for the enzymes from *Pyrococcus woesei* [10] and *Methanocaldococcus jannaschii* [12].

Of the 380 non-archaeal TIM sequences, 339 contain an aromatic residue at position 74 (126 Tyr, 206 Phe, 7 Trp and 22 His). At position 101, Tyr/Phe are observed in 180 sequences, and hydrophobic aliphatic residues (Ile/Leu/Val) are present in as many as 170 sequences. Similarly, at position 102, 223 sequences have Tyr/Phe and 96 have a His residue. Thus the aromatic cluster observed in *Pf*TIM is not a conserved feature in all the available sequences. Of the four aromatic residues that cluster at the dimer interface of TIM (Fig. 1), residue 69 is the most variable, being aromatic in only 13 of 380 sequences (including histidine at seven positions). The other three positions (74, 101 and 102) are more conserved, with aromatic/hydrophobic residues in 364 of 380 sequences.

Of the 32 TIM sequences available from archaea that form tetramers (not included in the 380 sequences), there is a deletion corresponding to positions 101 and 102, resulting in a restructuring of the dimer interface that appears to be necessary for the generation of the tetrameric TIMs. There is a resulting segregation between the archaeal sequences and bacterial and eukaryotic TIM sequences.

Interestingly, Trp is found at position 74 in seven of the non-archaeal sequences, and the crystal structure of
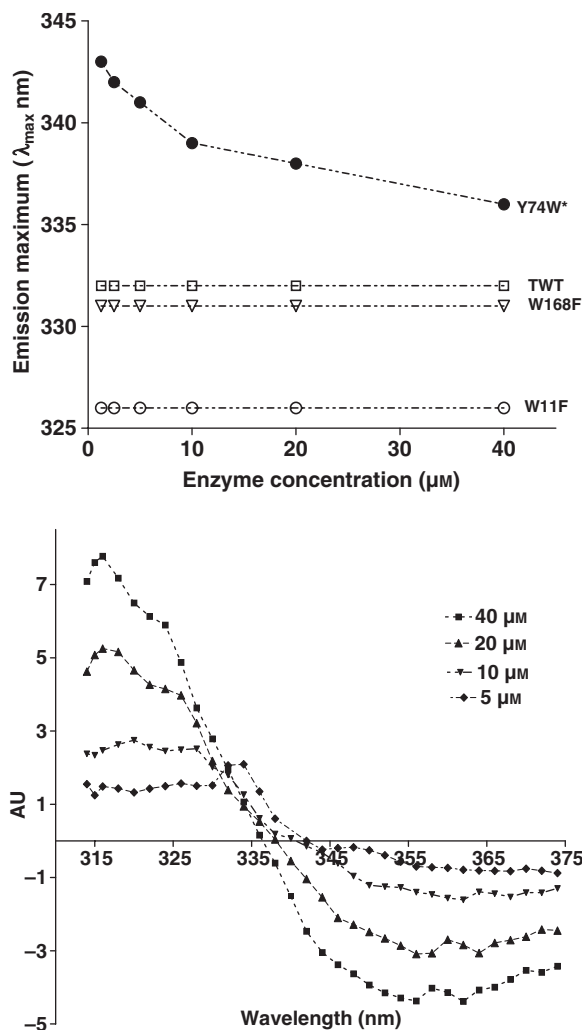
Fig. 4. Concentration-dependent shift in emission maxima for *Pf*TIM wild-type and single tryptophan mutants: the enzyme concentration range used was 40–1.25 µM (20 mM Tris/HCl pH 8.0). At higher concentration the mutant remains as a dimer. However, with dilution it shows monomer dimer equilibrium. With the increase of monomeric population the buried W74 gets exposed and its emission shifts towards higher wavelength. Top panel: comparison of the concentration dependence of fluorescence maxima for the enzymes TIM wild type (TWT), W11F, W168F and Y74W*. Bottom panel: first derivative of the fluorescence profile for Y74W* at various concentrations.

one member of this class is available, from *Giardia lamblia* [29]. A comparison of the immediate environment of residue 74 in the structures of TIMs from yeast, *P. falciparum* (*Pf*TIM) and *G. lamblia* (*Gl*TIM) reveals that the yeast and *Pf*TIM structures are very similar, although some subtle differences in aromatic ring orientation are evident. In contrast, *Gl*TIM, which contains Trp at position 75 (which is structurally equivalent to position 74 of *Pf*TIM), lacks other aromatic
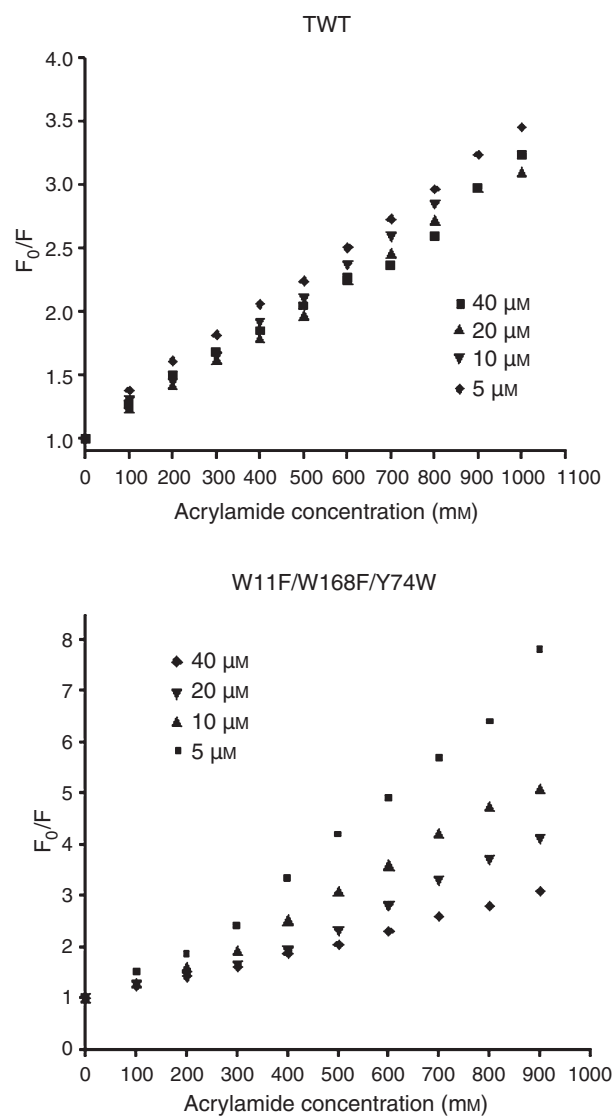
Fig. 5. Stern–Volmer plots showing concentration-dependent acrylamide quenching of tryptophan fluorescence for (A) TWT (emission at 332 nm) and (B) Y74W* (emission at 337 nm) at various protein concentrations. Quenching studies were performed in 20 mM Tris/HCl (pH 8.0).

rings in the vicinity. In comparing the three structures, it should be noted that the residue numbering is the same for the yeast enzyme and *Pf*TIM, but is increased by 1 in *Gl*TIM. Two features of the Y74W* mutant of *Pf*TIM need to be rationalized: (a) the reduced stability of the dimeric structure, and (b) the significantly lower value of k_{cat}, suggesting an impairment of the catalytic efficiency (k_{cat} for Y74W* = 0.06×10^5 min^{-1}; k_{cat} for *Pf*TIM WT* = 1.28×10^5 min^{-1}) (Table 2). With regard to stability, inspection of the data in Table 3 reveals that the triple mutant Y74W* has the lowest T_m value (37 °C) as determined by monitoring CD

ellipticity at 222 nm using a protein concentration of 20 μM. Under these conditions, the WT enzyme and all the other mutants listed in Table 3 show substantially higher values. The triple mutant also shows pronounced concentration dependence to gel filtration, consistent with subunit dissociation. With regard to impairment of the catalytic efficiency, it is notable that the K_m value of the triple mutant has not altered significantly even though the k_{cat} value is reduced 40-fold compared to WT and 20-fold compared to WT* (Table 2). k_2 (k_{cat}), which is the rate-limiting step in TIM catalysis, is much

Fig. 6. The neighborhood of residues (A) Y74 in *Pf*TIM (Protein Data Bank code 1O5X) and (B) W75 in *Gl*TIM (Protein Data Bank code 2DP3), and their interactions across the dimer interface. Relevant active site residues are also shown. The residue stretch 95–102 is also represented as a ribbon diagram. The residues in green are from subunit A and residues in cyan are from subunit B of dimeric triosephosphate isomerase.

slower than k_{-1} (dissociation of the enzyme–substrate complex) [32]. Thus the k_1/k_{-1} ratio is the actual determinant of K_m (binding affinity), and is not affected by the mutation.

Figure 6 shows the environment of residue 74, including the proximal residues of the TIM active site. The isomerization of dihydroxyacetone phosphate to glyceraldehyde 3-phosphate involves a proton abstraction from the substrate by the catalytic carboxylate of E165, followed by a proton transfer process to the enediol(ate) intermediate, completing the reaction cycle. While E165 and H95 have been postulated to be key residues involved in the catalytic process, K12 has also been implicated in substrate binding [33–36]. This key mechanistic insight into the TIM reaction derives from the seminal work of J.R Knowles and I. Rose [37–42]. Interestingly, mutation of the K12 residue results in a completely inactive enzyme, as evident from the studies of the K12M mutant of yeast TIM (k_{cat} = 1.08 min^{-1}, wild-type k_{cat} = 5.22 × 10^5 min^{-1}) [35]. A curious feature of the currently accepted mechanism for the TIM reaction is the involvement of the H95 residue as the imidazolate anion, despite the extremely unfavorable pK_a (approximately 14) for loss of a proton from neutral imidazole. Indeed Lodi and Knowles noted in 1992: 'Why the enzyme has evolved to use a neutral histidine as a general acid is not clear' [36]. Support for the postulated role of the neutral imidazole as an acid is derived from *ab initio* and molecular dynamics calculations [43]. However, Lodi and Knowles introduce a note of caution: 'Whether or not the details of this analysis will turn out to be correct, it is interesting that theory and experiment have agreed upon a result that runs counter to the initial prejudices of mechanistic chemistry' [34,44]. The residues K12, H95 and E165 are completely conserved in all available TIM sequences. E97 (see Fig. 6) is the fourth residue in the immediate neighborhood that is completely conserved and whose carboxylate group is within interaction distance for proton transfer from the ε-amino group of K12 and the imidazole of H95. A proton transfer process that involves all four residues may be envisaged in which H95 is either neutral or positively charged, eliminating the need to invoke an imidazolate at residue 95 [M. Banerjee, P. Balaram & N. V. Joshi (Centre for Ecological Sciences CES, IISC, Bangalore), unpublished results].

While precise mechanistic details are not central to the present discussion, it is interesting to note that three of the four completely conserved residues that lie close to the substrate binding site (K12, H95 and E97) are located in the vicinity of residue 74 (Fig. 6). Figure 7 show that Thr75, which is another completely conserved residue, forms key hydrogen bonding bonds

Fig. 7. Environment of Lys12 in the yeast TIM–dihydroxyacetone phosphate complex (Protein Data Bank code 1NEY), together with the dimer interface residues showing critical hydrogen bonds at the dimer interface. The residues in green are from subunit B and those in cyan are from subunit A. The active site residues of *P. falciparum*, yeast and *G. lamblia* TIMs superpose with an RMSD of approximately 0.8–1.2 Å.

through its backbone CO and NH groups to Arg98 and Glu97 of the neighboring subunit. The dimer interface and the network of hydrogen bond interactions positioning the active site residues are closely inter-connected. Taken together, Figs 6 and 7 suggest that dimerization is a prerequisite for construction of a catalytically competent active site. Subunit dissociation may thus be expected to result in a loss of enzymatic activity, as observed at low concentrations for the Y74W* mutant of *Pf*TIM. There have been several attempts to engineer monomeric TIMs, some of which retain the complete fold of the native enzyme [13,14]. However, the catalytic efficiencies of these engineered monomeric enzymes are reduced (k_{cat} for monoTIM = 312 min^{-1}; k_{cat} for wild-type TIM = 2.6×10^5 min^{-1}). Figure 7 shows that the residues N10 and Q64 form hydrogen bonds through their side chains to the backbone NH and CO groups of the completely conserved K12 residue. Of the 412 unique sequences (including archaeal sequences), the residues at position 10 (Asn) and position 64 (Gln) have been replaced by Ser in five sequences and Glu in 27 sequences, respectively. These replacements conserve the hydrogen bonding interactions shown in Fig. 7.

A notable feature of all TIM crystal structures reported to date is the conservation of the unusual backbone stereochemistry at the K12 residue. As shown in Fig. 8, K12 adopts unusual Ramachandran angles of $\phi = 54.3 \pm 5.5$ and $\psi = -144.1 \pm 7.0$ [53]. The distribution of the ϕ and ψ values of all other Lys residues in the TIM structure is shown for comparison. The possible role of energetically unfavorable Ramachandran disallowed conformations at enzyme active sites has been considered previously [45,46].

From Fig. 6A,B, it is evident that R98 is involved in key interactions with T75 across the dimer interface, while T75 interacts with N10 and E97 of the second subunit. The backbone NH group of R98 forms a hydrogen bond with the backbone CO of F102. Furthermore, the orientation of the side chain of the two residues brings the guanidinium plane and the aromatic ring of F102 into close proximity, with an almost perfectly parallel arrangement of the interacting groups (Fig. 9A). Interactions between guanidinium and aromatic residues have been suggested to be energetically stabilizing in both theoretical and experimental studies [47,48]. From Fig. 6, it is evident that the Y74W mutation in *Pf*TIM must necessarily result in displacement of the F102 side chain, with consequent effects on interactions involving R98.

Modeling studies indicated that insertion of a Trp residue at position 74 in the *Pf*TIM structure results in severe short contacts with neighboring residues in all possible rotameric states of the side chain. Thus, accommodation of a Trp residue at this position necessarily involves movement of proximal side chains. A cascade of side chain movements might then be expected to influence the precise positioning of the functional groups involved in catalysis, resulting in a significant reduction of k_{cat} values in the case of the Y74W* TIM mutant, even at concentrations at which the mutant enzyme exists solely in a dimeric form. Thus, restoration of the quaternary structure does not result in complete restoration of the catalytic efficiency. How does the *Gl*TIM accommodate the Trp residue at the equivalent position residue 75? Figure 6B shows a view of the environment of this residue that facilitates direct comparison with the *Pf*TIM structure shown in Fig. 6A. The residues that

Fig. 8. Key backbone hydrogen bonds between K12 and the side chains of N10 and Q64, which maintain the unusual Ramachandran angles for the K12 residue, and a Ramachandran scatter plot for the K12 residues in 21 TIM structures from various sources (available from the Protein Data Bank and including both free and inhibitor-bound structures). The K12 conformations are clustered in the lower right quadrant. The distribution of the ϕ and ψ values of all other Lys residues (total 1150) is shown for comparison. None of these Lys residues adopt the unusual backbone conformation seen for K12. The amino acid residues from the enzyme are shown in green. The substrate DHAP is shown in yellow.
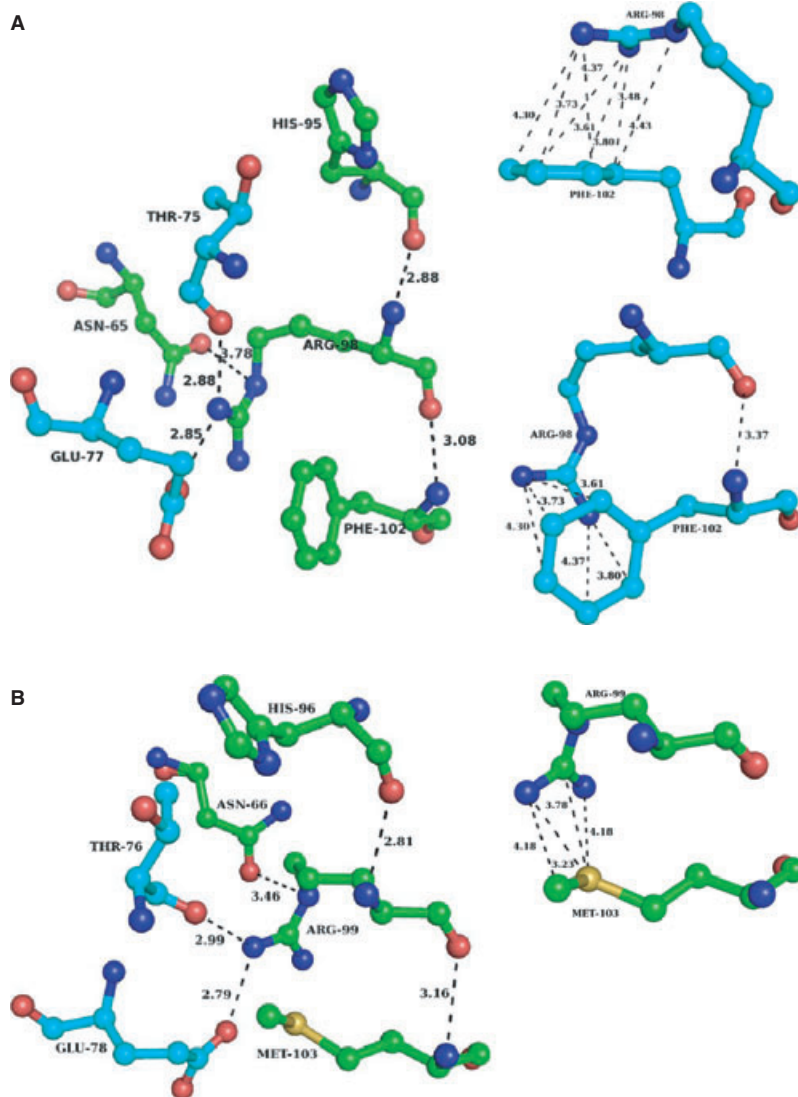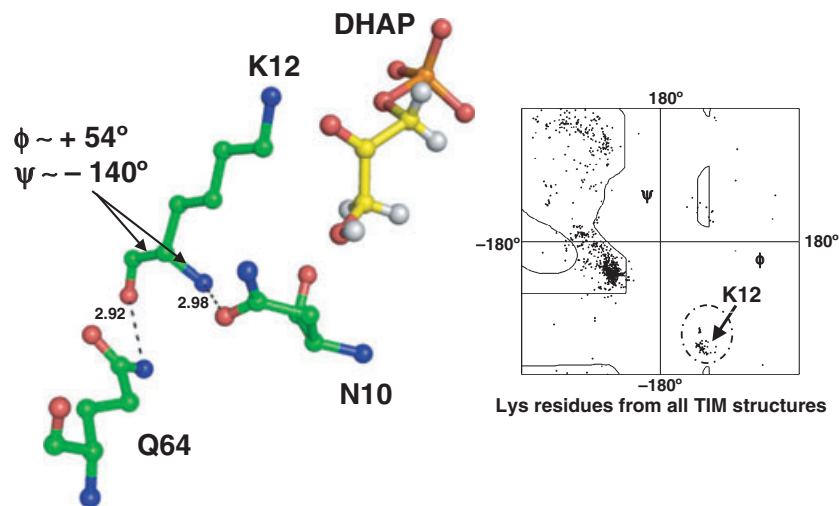
Fig. 9. The key interactions of a substantially conserved Arg residue (conserved in 353 of 380 sequences) with several residues near the active site and dimer interface. (A) Arg98 in *Pf*TIM (Protein Data Bank code 1O5X) and (B) Arg99 (the structural equivalent of Arg98 in *Pf*TIM) in *Gl*TIM (Protein Data Bank code 2DP3). The residues in green are from subunit A and residues in cyan are from subunit B of dimeric triosephosphate isomerase. Critical interactions between A′ and A″ [the guanidine group and aromatic residues of *Pf*TIM (R98/F102)] and the B′ guanidine and sulfur groups of *Gl*TIM (R99/M103) are marked.

face W75 (equivalent to residue Y74 in *Pf*TIM) across the dimer interface are the aliphatic residues I102 and M103. These mutations eliminate the steric crowding that would have occurred if aromatic residues had been positioned at these sites as in the case of TIMs from *Plasmodium* and yeast. Interestingly, the thioether group of M103 is positioned to make a potentially stabilizing contact with the guanidinium group of R99 (equivalent to R98 of *Pf*TIM and yeast TIM). The shortest distance from the sulfur atom of M103 to the NH1 nitrogen of the guanidium group of R99 is 3.23 Å, suggestive of a potentially stabilizing S-H-N interaction (Fig. 9B) [49].

The above discussion rationalizes the observed effects of the Y74W mutation in *Pf*TIM on the stability of the dimeric structure and catalytic activity. Examination of the available TIM sequences provides examples of where this mutation is indeed found in native enzymes. The availability of the enzyme from *G. lamblia* provides an opportunity to examine the nature of the complementary mutations employed in nature. The growing body of sequence and structural data on these well-studied enzymes affords an opportunity to evaluate the consequences of mutations. In the case of TIM, only nine of the 220–250 residues present in the sequences of the enzymes from diverse sources are indeed completely conserved. A relatively small number of positions accommodate only two or three possible amino acids (two substitutions are possible in five positions and three substitutions are possible in four positions). These positions include positions 10 and 64. Interestingly, the completely conserved positions and those exhibiting a very low diversity of substitution are all very close to the enzyme active site. This suggests that the driving force for evolutionary selection of protein sequences is the catalytic competence of the enzyme active site. The precise orientation of the functional residues is maintained by a network of interactions that severely limits the range of mutations that can be accommodated.

Experimental procedures

Site-directed mutagenesis

The wild-type *Pf*TIM gene was first cloned in the pTrc99A vector and expressed in AA200 *Escherichia coli* cells [50], which carry a null mutant of the TIM gene. For construction of the triple mutant Y74W* (W11F/W168F/Y74W), a tryptophan-less mutant W11F/W168F was used as a template. The W11F/W168F double mutant was generated on the W11F template. Briefly, the mutagenic primer was used together with the C-terminal primer *Pf*TIM to generate a mega primer containing the mutation. Site-directed mutagenesis was performed using the mega primer PCR method [51]. The primers used to make this mutant are listed in Table 1. In addition to the desired mutation, these primers also contained restriction sites, incorporated by silent mutagenesis, in order to aid selection of recombinants. The sites incorporated were *Hae*III, *Nco*I and *Bam*HI (Table 1). The PCR mix contained 200 ng of each primer, 20 ng of the template, 200 μM of each dNTP and 5 units of Taq DNA polymerase in a 50 μL reaction mixture. The PCR cycle used comprised denaturation at 94 °C for 4 min (hot start), then 93 °C for 25 s, annealing at 48 °C for 50 s and extension at 73 °C for 35 s. The product obtained after 30 cycles of PCR was purified by elution from agarose gels and used as a mega primer for the second round of PCR. The other primers used in the PCR amplification are listed in Table 1. The second PCR comprised 94 °C for 4 min (hot start), then 93 °C for 30 s, annealing at 52 °C for 50 s and extension at 73 °C for 1 min. After 30 cycles, a final extension of 10 min at 72 °C was performed. The full-length amplified product (746 bp) containing the desired mutation was purified using a gene cleaning kit (Qiagen, Qiagen India, Genetix Biotech Asia, New Delhi, India), digested with enzymes *Nco*I and *Bam*HI, and ligated into the vector pTrc99A, digested using the same enzymes. Recombinants were selected after transformation into *E. coli* strain DH5α on the basis of super-coiled plasmid mobility [51]. The presence of the correct insert was confirmed by restriction digestion using enzymes specific for the sites incorporated in the mutagenic primers. The triple mutant was constructed using the same procedure using the W11F/W168F mutant in the pTrc99A template. The primers Y74W* and TIM were used for the first round of mutagenesis in this case. The presence of mutations was confirmed by sequencing (Microsynth, Balgach, Switzerland), and the mutants were found to be free of PCR errors.

Protein expression and purification

Expression of the TIM gene was performed using the pTrc99A system. *E. coli* AA200 cells (containing a null mutant of the inherent TIM gene) carrying the pTrc99A

Table 1. Oligonucleotides used for site-directed mutagenesis.

Desired mutation	Template gene	Constructed mutant	Primer sequence (5′- to 3′)	Restriction site
W11F	WT	W11F	CA**CCATGG**CTAGAAAATATTTTGTCGCAGCAAACTTCAAATGTAA	*Nco*I
W168F	WT	W168F	GAACCTTTATTCGCTATT**GGTACC**GGTAAA	*Kpn*I
WT*	W11F	W11F/W168F	GAACCTTTATTCGCTATT**GGTACC**GGTAAA	*Kpn*I
Y74W*	WT*	W11F/W168F/Y74W	TCA**CCGG**TCCATGATCCATT	*Hae*III

Table 2. Comparison of kinetic parameters of *Pf*TIM interface mutants with those for wild-type *Pf*TIM, yeast and *Gl*TIM.

Enzymes	k_{cat} ($\times 10^5$ min^{-1})[a]	K_m (mM)	k_{cat}/K_m ($\times 10^5$ $min^{-1}·mM^{-1}$)	References
*Pf*TIM WT	2.68 ± 0.84	0.35 ± 0.16	7.65	[25]
*Gl*TIM	2.9 ± 0.2	0.53 ± 0.03	5.47	[29]
Yeast	1.41 ± 0.36	0.62 ± 0.05	0.54	[41]
W11F	1.55	0.41	3.78	[28]
W168F	1.57	0.30	5.23	[28]
W11F/W168F (WT*)	1.28 ± 0.37	0.45 ± 0.082	2.84	This study
Y74G	0.071 ± 0.016	0.34 ± 0.076	0.21	[25]
W11F/W168F/Y74W (Y74W*)[a]	0.06 ± 0.003	0.66 ± 0.04	0.09	This study

[a] The activity was measured at a protein concentration of 40 μM.

Table 3. Protein stability to chemical denaturants and temperature.

Enzymes	C_m urea (M)[a]	C_m guanidinium chloride (M)[a]	T_m (°C)[b]	Quaternary structure[c] (lowest concentration studied)	References
WT	> 8	2.4	58.0	Dimer (2.5 μM)	[25]
W11F	4.0	1.8	50	Dimer (2.5 μM)	[28]
W168F	> 8	2.0	55	Dimer (2.5 μM)	[28]
W11F/W168F[d]	3.4	1.2	44.8	Dimer (2.5 μM)	This study
Y74G	3.5	1.8	–	Dimer + monomer (20 μM)	[25]
W11F/W168F/Y74W (Y74W*)	2.9	0.9	37	Dimer + monomer (5 μM)	This study

[a] C_m is the mid-point of the unfolding profile monitored by CD (θ_{222} nm) and fluorescence (λ emission for $\lambda_{excitation}$ of 295 nm) over a denaturant concentration range of 0–8 M for urea and 0–7 M for guanidinium chloride. [b] T_m is the mid-point of thermal melting curve generated by monitoring CD ellipticity (θ_{222} nm). Irreversible protein precipitation occurs on thermal denaturation. [c] The column used for gel filtration was a Superdex-200 (length 30 cm, internal diameter 10 mm). Buffer containing 20 mM Tris/HCl (pH 8.0) with 100 mM sodium chloride was used for all runs at a flow rate of 0.5 mL·min^{-1}. [d] Protein denaturation was monitored only by change in CD ellipticity in the case of this tryptophan-less mutant.

recombinant vector were grown at 37 °C in terrific broth containing 100 μg·mL^{-1} ampicillin. Cells were induced using 300 μM isopropyl-β-D-thiogalactopyranoside until they reached an attenuance at 600 nm of 0.6–0.8, and were then harvested by centrifugation (15 min, 7245 *g* at 4 °C). Cells were resuspended in lysis buffer containing 20 mM Tris/HCl pH 8.0, 1 mM EDTA, 0.01 mM phenylmethanesulfonyl fluoride, 2 mM dithiothreitol and 10% glycerol, and disrupted using sonication. After centrifugation (45 min, 19 320 *g* at 4 °C), the protein fraction was precipitated with 60–80% ammonium sulfate. This precipitate was collected by centrifugation (30 min at 19 320 *g* at 4 °C) and re-suspended in buffer A (20 mM Tris/HCl pH 8.0, 2 mM dithiothreitol and 10% glycerol). Monitoring of each step was performed by SDS–PAGE analysis (12% polyacrylamide). Nucleic acid was removed by polyethylene-imine precipitation, and the subsequent purification steps were performed at 4 °C. The protein was dialyzed extensively against buffer A at 4 °C overnight, and purified using an anion exchange Q-Sepharose column (Amersham Biosciences, Uppsala, Sweden) eluted with a linear gradient of 0–1 M NaCl. The fractions containing the protein were pooled and precipitated by addition of ammonium sulfate to a concentration of 75%. The precipitated protein was dissolved in buffer A, subjected to gel filtration on a Sephacryl-200 column (Amersham Biosciences), equilibrated with the same buffer using an

AKTA Basic FPLC system (Amersham Biosciences). Protein purity was checked by 12% SDS–PAGE, and all samples were characterized by LC-ESI mass spectroscopy. Protein concentrations were determined by the Bradford method [53] using BSA as a standard.

Enzyme activity

The enzyme activity of TIM was determined by the conversion of glyceraldehyde 3-phosphate to dihydroxyacetone phosphate in the presence of TIM and α-glycerolphosphate dehydrogenase [54,55]. Enzymes were freshly prepared in 100 mM triethanolamine/HCl (pH 7.6). The reaction mixture (final volume 1 mL) contained 100 mM triethanolamine, 5 mM EDTA, 0.5 mM NADH and α-glycerolphosphate dehydrogenase (20 μg·mL^{-1}) and 0.10–3.0 mM glyceraldehyde 3-phosphate. Enzyme activity was determined by monitoring the decrease in absorbance of NADH at 340 nm. The dependence of the initial rate on the substrate concentration was analyzed according to the Michaelis–Menten equation (Eqn 1) as follows:

$$v = V_{max}[S]/K_m + [S] \tag{1}$$

where v and V_{max} are the initial velocity and the maximum velocity, respectively, K_m is the Michaelis constant, and S is the substrate concentration. The values for the kinetic

parameters (K_m, k_{cat}) were calculated from Lineweaver–Burke plots. The data were then analyzed using GRAPHPAD PRISM software, version 4.

Size-exclusion chromatography

Size-exclusion chromatography was performed using a Superdex-200 column (length 30 cm, internal diameter 10 mm) attached to an AKTA Basic HPLC system at a flow rate of 0.5 mL·min^{-1}. The solvent system was 20 mM Tris/HCl at pH 8.0. Protein elution was monitored at a wavelength of 280 nm. The column was calibrated using β-amylase (200 kDa), alcohol dehydrogenase (150 kDa), BSA (66 kDa), carbonic anhydrase (29 kDa) and cytochrome c (12.4 kDa). All chromatographic runs were performed at 25 °C.

Mass spectrometry

Electrospray ionization mass spectra were recorded on an electrospray mass spectrometer Esquire 3000$^+$ series (Bruker Daltonics) coupled to an online 1100 series HPLC (Agilent Technologies, Santa Clara, CA, USA). Nebulization was assisted by N$_2$ gas (99.8%) at a flow rate of 10 L·min^{-1}. The spray chamber was held at 300 °C. The spectrometer was tuned using five calibration standards provided by the manufacturer. Data processing was performed using the deconvolution module of the data analysis software to detect the multiple charge states and obtain derived masses.

Fluorescence spectroscopy

Fluorescence emission spectra were recorded on a Hitachi-250 spectrofluorimeter (Hitachi technologies, Tokyo, Japan). The protein samples were excited at 280 or 295 nm, separately, and the emission spectra recorded from 300–400 nm. Excitation and emission band passes were set at 5 nm. Denaturation studies were performed by incubating 10 μM protein with various concentrations of urea and guanidinium chloride for 45–60 min, and individual spectra were acquired from 300–450 nm after exciting the molecule at 295 nm. For quenching studies, acrylamide was added to the protein solution and incubated for 5 min, after which fluorescence spectra were recorded. The fluorescence intensities were normalized to construct the Stern–Volmer plots [30]. The excitation wavelength for quenching studies was 295 nm.

Circular dichroism (CD)

Far-UV CD measurements were performed on a JASCO-715 spectropolarimeter (JASCO technologies, Tokyo, Japan) equipped with a thermostatted cell holder. The temperature of the sample solution was controlled using a Peltier device. For thermal melting studies, ellipticity changes at 222 nm were monitored. A cuvette of path length 1 mm was used, and the spectra were averaged over four scans at a scanning speed of 10 nm·min^{-1}. The change in ellipticity was measured as a function of temperature for thermal melting. Denaturation studies were performed by incubating 4–5 μM protein with various concentrations of urea and guanidinium chloride for 45–60 min, and spectra (250–200 nm) are averaged over four scans.

Structure analysis

All structural superpositions were carried out by secondary structure matching using COOT [56]. Hydrogen bonds and van der Waals contacts were identified using the contact program of the CCP4 suite, based on distance criteria of 3.5 and 4.0 Å, respectively. The figures were generated using PYMOL [57].

Acknowledgements

References

1 Rieder SV & Rose IA (1959) The mechanism of the triosephosphate isomerase reaction. *J Biol Chem* **234**, 1007–1010.

2 Banner DW, Bloomer AC, Petsko GA, Phillips DC, Pogson CI, Wilson IA, Corran PH, Furth AJ, Milman JD, Offord RE *et al.* (1975) Structure of chicken muscle triosephosphate isomerase determined crystallographically at 2.5 Å resolution using amino acid sequence data. *Nature* **255**, 609–614.

3 Knowles JR (1991) Enzyme catalysis: not different, just better. *Nature* **350**, 121–124.

4 Putman SJ, Coulson AF, Farley IR, Riddleston B & Knowles JR (1972) Specificity and kinetics of triosephosphate isomerase from chicken muscle. *Biochem J* **129**, 301–310.

5 Phillips DC (1981) Crystallographic studies of movement within proteins. *Biochem Soc Symp* **46**, 1–15.

6 Rose IA (1981) Chemistry of proton abstraction by glycolytic enzymes (aldolase, isomerases and pyruvate kinase). *Philos Trans R Soc Lond B Biol Sci* **293**, 131–143.

7 Gracy RW (1982) Glucosephosphate and triosephosphate isomerases: significance of isozyme structural differences in evolution, physiology, and aging. *Isozymes* **6**, 169–205.

8 Lolis E & Petsko GA (1990) Transition-state analogues in protein crystallography: probes of the structural source of enzyme catalysis. *Annu Rev Biochem* **59**, 597–630.

9 Rodríguez-Almazán C, Arreola R, Rodríguez-Larrea D, Aguirre-López B, de Gómez-Puyou MT, Pérez-Montfort R, Costas M, Gómez-Puyou A & Torres-Larios A (2008) Structural basis of human triosephosphate isomerase deficiency: mutation E104D is related to alterations of a conserved water network at the dimer interface. *J Biol Chem* **283**, 23254–23263.

10 Walden H, Bell GS, Russell RJ, Siebers B, Hensel R & Taylor GL (2001) Tiny TIM: a small, tetrameric, hyperthermostable triosephosphate isomerase. *J Mol Biol* **306**, 745–757.

11 Walden H, Taylor GL, Lorentzen E, Pohl E, Lilie H, Schramm A, Knura T, Stubbe K, Tjaden B & Hensel R (2004) Structure and function of a regulated archaeal triosephosphate isomerase adapted to high temperature. *J Mol Biol* **342**, 861–875.

12 Gayathri P, Banerjee M, Vijayalakshmi A, Azeez S, Balaram H, Balaram P & Murthy MRN (2007) Structure of triosephosphate isomerase (TIM) from *Methanocaldococcus jannaschii*. *Acta Crystallogr D Biol Crystallogr* **63**, 206–220.

13 Borchert TV, Abagyan R, Kishan KV, Zeelen JP & Wierenga RK (1993) The crystal structure of an engineered monomeric triosephosphate isomerase, mono-TIM: the correct modelling of an eight-residue loop. *Structure* **1**, 205–213.

14 Borchert TV, Abagyan R, Jaenicke R & Wierenga RK (1994) Design, creation, and characterization of a stable, monomeric triosephosphate isomerase. *Proc Natl Acad Sci USA* **91**, 1515–1518.

15 Casal JI, Ahern TJ, Davenport RC, Petsko GA & Klibanov AM (1987) Subunit interface of triosephosphate isomerase: site-directed mutagenesis and characterization of the altered enzyme. *Biochemistry* **26**, 1258–1264.

16 Borchert TV, Zeelen JP, Schliebs W, Callens M, Minke W, Jaenicke R & Wierenga RK (1995) An interface point-mutation variant of triosephosphate isomerase is compactly folded and monomeric at low protein concentrations. *FEBS Lett* **367**, 315–318.

17 Schliebs W, Thanki N, Jaenicke R & Wierenga RK (1997) A double mutation at the tip of the dimer interface loop of triosephosphate isomerase generates active monomers with reduced stability. *Biochemistry* **36**, 9655–9662.

18 Mainfroid V, Terpstra P, Beauregard M, Frere JM, Mande SC, Hol WG, Martial JA & Goraj K (1996) Three hTIM mutants that provide new insights on why TIM is a dimer. *J Mol Biol* **257**, 441–456.

19 Ravindra G & Balaram P (2005) *Plasmodium falciparum* triosephosphate isomerase: new insights into an old enzyme. *Pure Appl Chem* **77**, 281–289.

20 Parthasarathy S, Ravindra G, Balaram H, Balaram P & Murthy MRN (2002) Structure of the *Plasmodium falciparum* triosephosphate isomerase – phosphoglycolate complex in two crystal forms: characterization of catalytic loop open and closed conformations in the ligand-bound state. *Biochemistry* **41**, 13178–13188.

21 Maithal K, Ravindra G, Balaram H & Balaram P (2002) Inhibition of *Plasmodium falciparum* triosephosphate isomerase by chemical modification of an interface cysteine: electrospray ionization mass spectrometric analysis of differential cysteine reactivities. *J Biol Chem* **277**, 25106–25114.

22 Gómez-Puyou A, Saavedra-Lira E, Becker I, Zubillaga RA, Rojo- Domínguez A & Pérez-Montfort R (1995) Using evolutionary changes to achieve species-specific inhibition of enzyme action studies with triosephosphate isomerase. *Chem Biol* **2**, 847–855.

23 Ostoa-Saloma P, Garza-Ramos G, Ramirez J, Becker I, Berzunza M, Landa A, Gomez-Puyou A, Tuena de Gomez-Puyou M & Perez-Montfort R (1997) Cloning, expression, purification and characterization of triosephosphate isomerase from *Trypanosoma cruzi*. *Eur J Biochem* **244**, 700–705.

24 Garza-Ramos G, Pérez-Montfort R, Rojo-Domínguez A, de Gómez-Puyou MT & Gómez-Puyou A (1996) Species-specific inhibition of homologous enzymes by modification of nonconserved amino acids residues. The cysteine residues of triosephosphate isomerase. *Eur J Biochem* **241**, 114–120.

25 Gokhale RS, Ray SS, Balaram H & Balaram P (1999) Unfolding of *Plasmodium falciparum* triosephosphate isomerase in urea and guanidinium chloride: evidence for a novel disulfide exchange reaction in a covalently cross-linked mutant. *Biochemistry* **38**, 423–431.

26 Gopal B, Ray SS, Gokhale RS, Balaram H, Murthy MR & Balaram P (1999) Cavity-creating mutation at the dimer interface of *Plasmodium falciparum* triosephosphate isomerase: restoration of stability by disulfide cross-linking of subunits. *Biochemistry* **38**, 478–486.

27 Maithal K, Ravindra G, Nagaraj G, Singh SK, Balaram H & Balaram P (2002) Subunit interface mutation disrupting an aromatic cluster in *Plasmodium*

falciparum triosephosphate isomerase: effect on dimer stability. *Protein Eng* **15**, 575–584.

28 Pattanaik P, Ravindra G, Sengupta C, Maithal K, Balaram P & Balaram H (2003) Unusual fluorescence of W168 in *Plasmodium falciparum* triosephosphate isomerase, probed by single-tryptophan mutants. *Eur J Biochem* **270**, 745–756.

29 Reyes-Vivas H, Diaz A, Peon J, Mendoza-Hernandez G, Hernandez- Alcantara G, De la Mora-De la Mora I, Enriquez-Flores S, Dominguez-Ramirez L & Lopez-Velazquez G (2007) Disulfide bridges in the mesophilic triosephosphate isomerase from *Giardia lamblia* are related to oligomerization and activity. *J Mol Biol* **365**, 752–763.

30 Lakowicz JR (1999) *Principles of Fluorescence Spectroscopy*, 2nd edn. Plenum Press, Nw York.

31 Jogl G, Rozovsky S, McDermott AE & Tong L (2003) Optimal alignment for enzymatic proton transfer: structure of the Michaelis complex of triosephosphate isomerase at 1.2 Å resolution. *Proc Natl Acad Sci USA* **100**, 50–55.

32 Albery WJ & Knowles JR (1976) Free-energy profile of the reaction catalyzed by triosephosphate isomerase. *Biochemistry* **15**, 5627–5631.

33 Raines RT & Knowles JR (1986) The mechanistic pathway of a mutant triosephosphate isomerase. *Ann NY Acad Sci* **471**, 266–271.

34 Nickbarg EB, Davenport RC, Petsko GA & Knowles JR (1988) Triosephosphate isomerase: removal of a putatively electrophilic histidine residue results in a subtle change in catalytic mechanism. *Biochemistry* **27**, 5948–5960.

35 Komives EA, Chang LC, Lolis E, Tilton RF, Petsko GA & Knowles JR (1991) Electrophilic catalysis in triosephosphate isomerase: the role of histidine-95. *Biochemistry* **30**, 3011–3019.

36 Lodi PJ, Chang LC, Knowles JR & Komives EA (1994) Triosephosphate isomerase requires a positively charged active site: the role of lysine-12. *Biochemistry* **33**, 2809–2814.

37 Hall A & Knowles JR (1975) The uncatalyzed rates of enolization of dihydroxyacetone phoshate and of glyceraldehyde 3-phosphate in neutral aqueous solution. The quantitative assessment of the effectiveness˜of an enzyme catalyst. *Biochemistry* **14**, 4348–4353.

38 Albery WJ & Knowles JR (1976a) Evolution of enzyme function and the development of catalytic efficiency. *Biochemistry* **15**, 5631–5640.

39 Leadlay PF, Albery WJ & Knowles JR (1976) Energetics of triosephosphate isomerase: deuterium isotope effects in the enzyme-catalyzed reaction. *Biochemistry* **15**, 5617–5620.

40 Albery WJ & Knowles JR (1977) Efficiency and evolution of enzyme catalysis. *Angew Chem Int Ed Engl* **16**, 285–293.

41 Rose IA (1984) Failure to confirm previous observation on triosephosphate isomerase intermediate and bound substrate complexes. *Biochemistry* **23**, 5893–5894.

42 Rose IA, Fung WJ & Warms JV (1990) Proton diffusion in the active site of triosephosphate isomerase. *Biochemistry* **29**, 4312–4317.

43 Bash PA, Field MJ, Davenport RC, Petsko GA, Ringe D & Karplus M (1991) Computer simulation and analysis of the reaction pathway of triosephosphate isomerase. *Biochemistry* **30**, 5826–5832.

44 Cui Q & Karplus M (2003) Catalysis and specificity in enzymes: a study of triosephosphate isomerase and comparison with methyl glyoxalsynthase. *Adv Protein Chem* **66**, 315–372.

45 Gunasekaran K, Ramakrishnan C & Balaram P (1996) Disallowed Ramachandran conformations of amino acid residues in protein structures. *J Mol Biol* **264**, 191–198.

46 Jia Z, Vandonselaar M, Quali JW & Delbaere TJ (1993) Active-centre torsion-angle strain revealed in 1.6 Å-resolution structure of histidine-containing phosphor carrier protein. *Nature* **361**, 94–97.

47 Dougherty DA (2007) Cation–π interactions involving aromatic amino acids. *J Nutr* **137**, 1504S–1508S.

48 Crowley P B & Golovin A (2005) Cation–π interactions in protein interfaces. *Proteins* **59**, 231–239.

49 Gregoret LM, Rader SD, Fletterick RJ & Cohen FE (1991) Hydrogen bonds involving sulfur atom in proteins. *Proteins* **9**, 99–107.

50 Ranie J, Kumar VP & Balaram H (1993) Cloning of the triosephosphate isomerase gene of *Plasmodium falciparum* and expression in *Escherichia coli*. *Mol Biochem Parasitol* **61**, 159–169.

51 Sarkar G & Sommer SS (1990) The 'megaprimer' method of site-directed mutagenesis. *BioTechniques* **8**, 404–407.

52 Sambrook J & Russell DW (2001) *Molecular Cloning: A Laboratory Manual*, 3rd edn. Cold Spring Harbor Laboratory Press, Cold Spring Harbor, NY.

53 Bradford MM (1976) A rapid and sensitive method for the quantitation of microgram quantities of protein utilizing the principle of protein–dye binding. *Anal Biochem* **72**, 248–254.

54 Oesper P & Meyerhof O (1950) The determination of triose phosphate isomerase. *Arch Biochem* **27**, 223–233.

55 Plaut B & Knowles JR (1972) pH-dependence of the triosephosphate isomerase reaction. *Biochem J* **129**, 311–320.

56 Krissinel E & Henrick K (2004) Secondary-structure matching (SSM), a new tool for fast protein structure alignment in three dimensions. *Acta Crystallogr D Biol Crystallogr* **60**, 2256–2268.

57 DeLano WL (2002) *The PyMOL Molecular Graphics System*. DeLano Scientific, San Carlos, CA.

Supporting information

The following supplementary material is available:

Fig. S1. Reducing 12% SDS–PAGE for purified *Pf*TIM wild-type and mutants.

Fig. S2. LC-ESI mass spectra of *Pf*TIM W11F/ W168F and W11F/W168F/Y74W mutants, together with its charge state distribution.

Fig. S3. Michaelis–Menten and Lineweaver–Burke plots of *Pf*TIM interface mutants.

This supplementary material can be found in the online version of this article.

Please note: As a service to our authors and readers, this journal provides supporting information supplied by the authors. Such materials are peer-reviewed and may be re-organized for online delivery, but are not copy-edited or typeset. Technical support issues arising from supporting information (other than missing files) should be addressed to the authors.